X-621-77-268

TM-78056

MERCURY'S HELIUM EXOSPHERE AFTER MARINER 10's THIRD ENCOUNTER

S. A. CURTIS
R. E. HARTLE

NOVEMBER 1977

GSFC
GODDARD SPACE FLIGHT CENTER
GREENBELT, MARYLAND

X-621-77-269

MERCURY'S HELIUM EXOSPHERE AFTER MARINER 10's THIRD ENCOUNTER

S. A. Curtis and R. E. Hartle

November 1977

GODDARD SPACE FLIGHT CENTER
Greenbelt, Maryland

CONTENTS

LIST OF TABLES

LIST OF FIGURES

LIST OF FIGURES

MERCURY'S HELIUM EXOSPHERE AFTER MARINER 10's THIRD ENCOUNTER

S. A. Curtis and R. E. Hartle
Laboratory for Planetary Atmospheres

ABSTRACT

From a comparison of the Mariner 10 third encounter UV spectrometer data with intensities generated from a newly constructed model exosphere, we have derived a new value of 4.5×10^{-4} for the fraction of the solar wind He^{++} flux to be intercepted and captured by Mercury's magnetosphere if the observed He atmosphere is maintained by the solar wind. If an internal source for He prevails, the corresponding upper bound for the global outgassing rate is estimated to be 4.5×10^{22} sec^{-1}. These values differ from those given earlier due to the present use of a surface temperature distribution satisfying the heat equation over Mercury's entire surface which employs Mariner 10 determined mean surface thermal characteristics. We also use the mean stand off distance of Mercury's magnetopause averaged over Mercury's orbit. We find the agreement between the observed and calculated intensities to be good and believe that the minor discrepancies that exist on the nightside of the

ABSTRACT

terminator are explicable in terms of differences between actual and computed surface temperatures and the resulting scale height structure changes. We attribute these temperature differences to the inhomogeneity of the physical properties of the surface of Mercury.

MERCURY'S HELIUM EXOSPHERE AFTER MARINER 10's THIRD ENCOUNTER

INTRODUCTION

As a result of Mariner 10's three encounters with Mercury, the prevailing view of the relationship between the atmosphere and the solar wind has changed dramatically. A review of the observations and interpretation of Mercury's atmosphere has been presented by Kumar (1976). Our interest here lies primarily in the interpretation of the third encounter observations of the He atmosphere at Mercury's evening terminator (Broadfoot et al., 1976a). We will compare our theoretical 584 Å intensities to the intensities observed by Mariner 10 in order to ascertain the validity of the model's assumptions concerning the He atoms' accommodation with local surface conditions. Our investigation is constrained by uncertainties in the derived surface temperature due to inhomogeneities in the surface properties. We will show that the data appear to support the model's assumptions to a degree which allows new updated estimates of the total fraction of solar wind He^{++} captured by the Hermian magnetosphere and which impacts the planet's surface, maintaining the observed He exosphere solely by this external source. Also, a new upper bound to the total surface outgassing rate will be given.

Pre-encounter models (Hartle, et al., 1973; Hodges, 1974) assume a direct interaction of the ambient solar wind with the Hermian surface. In those models the solar wind provided the source for the atmosphere, and its magnitude was

determined by the solar wind flux intercepted by Mercury. The Mariner 10 encounters discovered that direct solar wind interaction was generally not possible, since Mercury was found to possess a magnetosphere (Ness et al., 1974; Ogilvie et al., 1974). This magnetosphere deflects most of the solar wind from Mercury under typical solar wind conditions (Siscoe and Christopher, 1975). The encounter measurements also revealed a He atmosphere (Broadfoot et al., 1974). From encounter measurements Hartle et al. (1975) constructed a model to account for the observed magnetospheric shielding of Mercury's surface from the solar wind. The model indicated the observations implied a tenuous He atmosphere which is collisionless down to the planet's surface and hence is an exosphere. From the model, preliminary estimates were made for the magnetospheric capture fraction of solar wind He^{++} required to maintain the observed He exosphere. In addition, an upper bound for the surface outgassing rate required to maintain the He exosphere was also obtained from the model. For simplicity, the early model assumed a surface temperature distribution based on radiative equilibrium. This assumption led to a good approximation of the temperatures over most of the dayside, but was not appropriate near the evening and morning terminators (Hartle et al., 1975). The need for a more realistic temperature distribution is evident from the Mariner 10 third encounter UV observations of the sensitive terminator region (Broadfoot et al., 1976a). A minimum requirement for a surface temperature distribution in the present case would be for it to satisfy the heat equation over the entire Hermian surface using the surface thermal properties determined

by Mariner 10 (Chase et al., 1976). The differences in global parameters such as total atmospheric content are not large when the temperatures are determined from either the radiative equilibirum condition or the heat conduction equation. However, the localized UV measurements of Mariner 10 are extremely sensitive to the terminator temperature distribution and hence a very realistic temperature model is needed if theory is to be quantitatively compared with experiment in this region (Hartle et al., 1975).

METHOD & CALCULATION

In this section we discuss in detail the three stages of calculations that are necessary in order to generate a model helium exosphere for Mercury from which detailed comparisons with Mariner 10 encounter UV observations are possible. The first of these stages is the calculation of the surface temperature distribution, obtained by solving the heat conduction equation over the planet's surface. The second stage incorporates the surface temperature distribution into a Monte Carlo model for the surface helium exobase density normalized by a constant factor. The third and final stage involves a solution of the collisionless Boltzmann equation for the global He density distribution in the exosphere, where the highly non-uniform exobase temperatures and densities provide the needed boundary conditions. We now elaborate on each of the three parts of the model generation.

In calculating the exobase temperature, $T(z,t)$, we solve the heat conduction equation (Richtmyer, 1962), assuming a homogeneous surface

$$\rho c \frac{\partial T(z,t)}{\partial t} = K \frac{\partial^2 T(z,t)}{\partial z^2} \qquad (1)$$

where ρ is the surface density, c is the specific heat capacity, K is the thermal conductivity, t is the time and z is the distance below Mercury's surface. In solving (1) we applied the following boundary conditions:

$$K \left.\frac{\partial T(z,t)}{\partial z}\right|_{z=0} = \epsilon\sigma T^4 (z=0,t) - (1-a)\Gamma(t) \tag{2}$$

$$K \left.\frac{\partial T(z,t)}{\partial z}\right|_{z=z_0} = 0 \tag{3}$$

where ϵ is the emissivity, σ is the Stephan-Boltzmann constant, a is the albedo, and z_0 is the depth of the bottom of the slab in which the solution is sought. $\Gamma(t)$ is the solar insolation as determined from Mercury's ephemeris. In (1) and (3) we have neglected the heating contribution due to radioactive decay of uranium and thorium in the Hermian interior as it is negligible in the case of a uniform source of decay under the planet's surface. If, however, the sources of radioactive decay are highly non-uniform, then local hot spots may be produced on the night side. The deviations between such hot spots and the uniform temperature model would be similar to those deviations caused by higher thermal inertias than the uniform value assumed. In Table 1 we give the values of the above parameters used in the solution. The values characterizing the Hermian surface are taken from those adopted by the IR team from their radiometer observations (Chase et al., 1976). The details of the numerical analysis of (1), subject to (2) and (3) as well as the analytical form of $\Gamma(t)$ have been discussed extensively (Linsky, 1965; Ingrao et al., 1965; Linsky, 1966; Morrison, 1969; Morrison, 1970). In solving

(1) we have chosen a grid with a time increment $\Delta t \approx 1$ earth day and a corresponding depth increment $\Delta z \approx 3$ cm as necessitated by stability requirements. We chose as a first guess to the solution the radiative equilibrium solution we employed earlier (Hartle et al., 1975). We note however that particular care must be taken in numerically solving (1) by the methods cited. Specifically, the solution is prone to oscillatory problems that can destroy the convergence in the low temperature gradient regions on the night side and in areas with very low solar insolation near the terminators at higher latitudes. The tendency is to overshoot the true solution. To eliminate this problem we apply a dampening factor to the computed change of the surface temperatures at each iteration step in these oscillation prone regions. We then obtain a smooth convergence with an estimated precision of approximately 1°K. The iteration is performed over multiples of two Hermian years (two orbital periods), the time over which a surface point experiences a complete solar insolation cycle. The insolation received by the aphelion subsolar point and its resulting temperature response is shown in Figure 1 for the complete two Hermian year ($\approx$176 earth days) solar insolation cycle. The unusual form of the insolation is derived from the 3/2 spin-orbit resonance of Mercury and its relatively high orbital eccentricity. Although we have derived the exobase temperature distribution over the entire Hermian solar insolation cycle, our interest here is restricted to the aphelion temperatures at the time of the Mariner 10 encounters. In Figure 2 we give the aphelion exobase surface temperatures $T(\lambda, \phi)$ as functions of latitude λ, and longitude ϕ, with $\phi = 0°$

representing the noon meridian and $\lambda = 0°$ the equator. In Figures 2b-c we show cross sections of this contour plot at low and high latitudes with the horizontal axis scaled by $\cos\lambda$ in order to give the reader a feeling for the longitudinal temperature gradients (circumference $\propto \cos\lambda$). As is readily apparent from these two figures, there is a marked asymmetry between the morning and evening terminators with the smaller evening temperature gradients corresponding to night time cooling and the morning temperature gradients being quite steep due to the step function-like turn on of the solar insolation at sunrise. Also, for large distances about the subsolar point on the dayside, the solution is very nearly that given by radiative equilibrium with $T(\lambda, \phi) = 575\ [\sin\lambda\ \cos\phi]^{1/4}$°K. The surface temperature on Mercury has perhaps the largest contrast in the solar system. At aphelion it spans temperatures from a nightside pole value of ≈ 80°K to a subsolar value of ≈ 575°K.

We use the aphelion exobase temperature described above to generate the exobase helium density distribution. The method we employ is a Monte Carlo technique wherein single He atoms are followed over the planet's surface until they either escape thermally or, as is less likely, are ionized and picked up by the surrounding magnetosphere. The details of the calculation have been presented in an earlier paper (Hartle et al., 1975). The resulting aphelion exobase He density distribution $n(\lambda, \phi, z=0)$, normalized by the subsolar point density n_0, is shown in Figure 3a. In Figures 3b-c we display cross sections of Figure 3a at low and high latitudes, with the horizontal (ϕ) axis scaled by $\cos\lambda$ in order to

in order to accurately show the longitudinal surface density gradients. The signature of the exobase density response to the exobase temperature distribution is apparent from the steeper gradients in the morning than in the evening. We note, however, that non-local effects of a global nature are also apparent from an inspection of Figures 3a-c. The maximum density bulge occurs off the equator and marks the most effective trapping region for helium on the nightside. The effectiveness of the trapping is determined both by how cold it is and the extent of the cold region on the surface. These effects combine to determine the length of time an atom will spend ballistically hopping around in a given region and hence gives a measure of how long it remains trapped. Thus the maximum density does not appear near the poles which are the coldest areas on the planet nor does it occur at the equator which has the largest low temperature region. Rather, the maximum density occurs in between, where both of these characteristic trapping parameters combine to form the best trap. The smallness of the polar trapping region is readily apparent from both Figures 2a-c and 3a-c. Most of the nightside structure seen in Figure 3a can be attributed to global processes and not the relatively featureless local nightside exobase temperatures of Figure 2a.

Using the exobase temperatures and He exobase densities described above, our model Hermian exosphere is generated directly as a solution to the collisionless Boltzmann equation with these exobase distributions as boundary conditions. The details of the method of solution of this equation for nonuniform planetary

exobase conditions is given by Hartle (1971). Rather than computing the entire exosphere we have, for reasons of economy, restricted our calculations to those necessary to compute the column densities needed for comparison with the Mariner 10 third encounter UV observations. The column densities which we compute are of the form

$$\eta = \int_{s_0}^{s_c} \frac{n}{n_0} \, ds \tag{4}$$

where s_0 is the intersection of the viewing direction with the planet when such an intersection exists (for views across the limb $s_0 = -\infty$), and s_c is the spacecraft position at the time of viewing. The instrument viewing slit (Broadfoot et al., 1976b) is divided into segments and for each segment a column density of the form of (4) is computed. The integrated contribution of these segments for a given slit (accounting for the instrument's transmission function) gives the normalized intensity seen by each slit. In order to determine the normalization factor for our computed intensities, they are renormalized to those measured off the dayside limb by Broadfoot et al. (1976a). In Figure 4 we compare the resulting renormalized model intensities with the Mariner 10 measured He 584 Å intensities. The plot is conveniently broken into three parts. These parts are: (1) the region off the dayside limb which shows very good agreement with the model, (2) the region between the dayside limb and the terminator which shows the observed intensities exceeding the model by a large amount due to surface scattering of 584 Å radiation off the planet's surface, and (3) the region to the nightside of the terminator which follows the data but shows some discrepancies.

DISCUSSION

Returning to Figure 4, we note the agreement with the observations is good off the dayside limb (region 1) as is expected since radiative equilibrium holds on the surface there and thus the local temperatures are nearly independent of the local thermal properties of the soil. In contrast, there are notable differences on the nightside of the terminator (region 3). The large differences between model and data in the intermediate region 2 are attributed to Mercury's UV surface albedo. We find these night side (region 3) discrepancies to be much less than those calculated from a model exosphere by Broadfoot et al. (1976a), wherein a large excess of density was derived in this region. From Figure 4 the nature of these differences in region 3 are seen to be like a phase shift of the model intensities to later local times with respect to the observed intensities. We suggest the nightside differences near the terminator are due to the extreme sensitivity of the intensities to the surface temperatures in this region of large longitudinal temperature gradients. The temperatures themselves are sensitive to the local thermal parameters and hence will reflect soil inhomogenities. This sensitivity arises from the location of the exospheric densities contributing most to the observed intensities. Such densities are generally located at several scale heights

$$H = R_{\mathbb{Q}} / \alpha \tag{5}$$

above the surface of Mercury, where $R_{\mathbb{Q}}$ is the Hermian radius and

$$\alpha = \frac{GM_{\mathbb{Q}}\, m}{R_{\mathbb{Q}}\, kT(\lambda,\phi)} \tag{6}$$

is a measure of the He atoms ratio of gravitational potential energy to kinetic energy in terms of the gravitational constant G, the mass of Mercury $M_{\mathbb{Q}}$, the He atom's mass m and Boltzmann's constant k. The terminator region is characterized by H ~50-100 km. Surface densities do not contribute to the observed intensities here due to the shadow of Mercury that blocks light to this surface region. The densities in this night region are well approximated by the barometric law

$$n(\lambda,\phi) = n(\lambda,\phi, z=0) \exp\left[\frac{-\alpha z}{R_{\mathbb{Q}}}\right] \tag{7}$$

We note that if there exists an error δT in the exobase temperature, not only is the base density distribution modified, but the height distribution is nonlinearly altered with α being replaced by $\alpha' = \frac{\alpha}{1+\frac{\delta T}{T}}$. Thus, if the actual temperature at the exobase is lower than that calculated from the heat equation, α' will increase, H will decrease and the density will decline more rapidly with height, resulting in lower column densities and intensities. To be more quantitative, consider the fractional change in density at height z caused by a difference between model temperatures, T_m, and actual temperatures T_A of $\delta T = T_A - T_m$:

$$\frac{\Delta n}{n} = \left[1-\left(\frac{\delta T}{T}\right)^3\right] \exp\left[\frac{\alpha z}{R_{\mathbb{Q}}} \frac{\delta T}{T}\right] - 1 \tag{8}$$

where we have used the fact that the exobase densities vary with the exobase temperatures roughly as T^{-3}. This density variation with temperature is deduced from the minimization of

$$\delta(x) = \frac{\iint ds \left(\frac{nT^x}{n_o T^x{}_o} - 1 \right)^2}{\iint ds}$$

where the integration is over the Hermian surface. We solve the equation iteratively for x such that $\delta(x) << 1$ and find $x = 3.166 \pm .002$. For purposes of illustration here we will simply use $x = 3$. Now we consider the case in which $\delta T < 0$. In particular, from Chase et al. (1976) in their Figure 6 we note that there is a large deviation between model temperatures and observations near 1800 Mercury local time; i.e., near the evening terminator. Specifically, with a thermal inertia of 0.0020 cal cm^{-2} $sec^{-1/2}$ $°K^{-1}$ similar to that adopted in our temperature calculations and with the same type of temperature model, deviations, $\left|\frac{\delta T}{T}\right| > 0.2$ appear to be implied. Using the value $\frac{\delta T}{T} = -0.2$ the fractional deviation $\frac{\delta n}{n}$ at 2 scale heights above the surface is $\sim -.45$. Thus the model would appear to overestimate the density by almost a factor of two. We conclude from these remarks that the non-linear amplification of model-actual temperature difference effects via the scale height dependence of the column density contributions can explain the observed phase shift-like differences in the terminator region. We attribute the temperature differences to the idealization made in regarding the Hermian surface as homogeneous and uniform in terms of its thermal parameters. The sensitivity of the surface temperature to these assumptions is readily seen from Figures 6 and 7 of Chase et al. (1976). We emphasize here that the measurements made in the terminator region are indirect indications of the magnitude of

the large nightside densities, similar to those measured directly on the Moon by means of a surface mass spectrometer (Hodges and Hoffman, 1974). It would appear that by such direct in situ measurements of density a separation of nightside temperature and densities could be much more precisely obtained. A similar, although less precise, separation could be made if the temperatures were measured globally by an orbiting satellite allowing the construction of an empirical temperature model reflecting the surface inhomogeneities. This model coupled with UV intensity observations would separate densities and temperatures better than the current encounter measurements of Mariner 10. The differences between the homogeneous model intensities and the Mariner 10 observations have been taken by Broadfoot et al. (1976a) to indicate departures from the surface physics assumed by these models (Hodges, 1974; Hartle et al., 1975). From the results obtained here we feel that for the specific case of helium on Mercury such deviations could well be small since the deviations from homogeniety of the surface thermal properties as determined from the Mariner 10 IR experiment (Chase et al., 1976) appear to account for the differences between model and UV data intensities. A determination of any non-negligible surface physics deviations would require more detailed measurements as discussed earlier.

From the preceding comparison of the Mariner 10 UV results for atomic helium and our model, we conclude that the agreement is sufficiently good so as to allow a calculation of the total atmospheric content. We are then able to estimate the capture fraction of solar wind He^{++} of the Hermian magnetosphere needed

to maintain the observed atmosphere. In the opposite limit, we also compute an upper bound for the Hermian outgassing rate presumably for an internal radiogenic source. In calculating the total atmospheric content, N_T, we integrate over a semi-infinite shell containing the Hermian surface

$$N_t \approx = R_+^2 \int_0^{\infty} dz \int_{-1}^{+1} du \int_0^{2\pi} d\phi \qquad n(u,\phi,z)$$

where $u = \cos\lambda$. We find N_T to be well approximated by

$$N_T \approx R^2 \int_{-1}^{1} du \int_0^{2\pi} d\phi \, H(u,\phi),\, n(u,\phi,z=0)$$

where $H(u, \phi)$ is the local scale height. The resulting total exospheric content we compute is $N_T = 6 \times 10^{29}$ He atoms. This value of N is less than that determined earlier (Hartle et al., 1975) due to the enhanced post sunset evening temperatures of the heat conduction equation solution as shown in Figure 2. These are to be contrasted with the pre-dawn morning temperatures which closely follow the radiative equilibrium solution. The resulting evening density depletion of Figure 3 reduces the total nightside density by ~.3. As the night side density bulge is almost the entire content of the exosphere, the total atmosphere content is reduced by a corresponding amount. Also from a comparison of model intensities to observed intensities we derive a subsolar point density of $n_o = 1 \times 10^3$ atoms cm^{-3}. In obtaining n_o we have used the relation

$$n_o = \frac{I}{g\eta} \tag{10}$$

in terms of the currently accepted value of g-factor (Broadfoot et al., 1975a), where I is the observed intensity and η is the computed model column density

from equation (4). This value of n_o is in agreement with our previously reported value (Hartle et al., 1975) when the differences in observed intensities between Mariner 10 encounter I and encounter III are accounted for. This is to be expected since n_o is determined off the dayside limb whose surface temperature is nearly independent of soil thermal properties. Our present value of n_o does differ substantially from that calculated by Broadfoot et al. (1976a) of 4.5×10^3 cm^{-3}. Comparing their Figure 2 to our Figure 4 we note that off the dayside limb the Broadfoot model is consistently above the data whereas our model tracks the data quite well in this region. If the Broadfoot et al. model is normalized to ours just off the limb, their value of n_o becomes 2.5×10^3 cm^{-3}, in agreement with the value presented here. We now proceed to calculate the capture fraction, f_c, required for the He exosphere's maintenance. Siscoe and Christopher (1975) have discussed the dependence of the solar wind stand off distance, r_{st}, at Mercury as determined from the balance of solar wind pressure and the Hermian magnetic dipole field pressure. From their values of r_{st} at aphelion and perihelion, the dependence of the dipole magnetic field pressure, $B^2_{st/8\pi}$, on r_{st} and the dependence of the solar wind density on solar distance R via the continuity equation for solar wind He^{++}, we find that the capture cross section, σ_{sc}, varies as

$$\sigma_{sc} = 6.65\pi R_\odot^2 \; R^{2/3} \; \delta \tag{11}$$

where δ is a geometrical factor which is the squared ratio of the magnetopause distance at 90° to the standoff distance $\delta = (r_{st}(90°)/(r_{st}(0°))^2$ and R is in AU. From

Figure 2 of Ness et al. (1975) one obtains an estimate of $\delta = 1.60$. Now the mean residence time τ of an He atom on Mercury, before it is lost by an escape process is $\sim 1.3 \times 10^7$ sec slightly less than the value reported earlier (Hartle et al., 1975). This is on the order of the temperature cycle period of 2 Hermian years. We thus expect the total He exospheric content to be approximately constant with variations in the exobase temperatures affecting the shape of the exobase density distribution. We can then write

$$\frac{N_T}{\tau} = 6.65\pi\, n_0 v_0 < R^{-4/3} >_{orbit} \; R_\mu^2 \; f_c \qquad (12)$$

where $n_0 u_0 = 1.5 \times 10^7$ He^{++} cm^{-2} sec^{-1} is the solar wind flux at 1 AU. The $R^{-4/3}$ dependence reflects both the radical dependence of the solar wind flux on distance (R^{-2}) and that of the capture cross section ($R^{2/3}$). The bracket $< >_{orbit}$ represents an average over the Hermian orbit,

$$< R^{-4/3} >_{orbit} = .562 \int_0^{2\pi} d\theta \, [1+.206 \cos\theta]^{-2/3} \qquad (13)$$

From (13) and (12) we obtain $f_c \approx 4.5 \times 10^{-4}$ as the Hermian magnetosphere's capture fraction. The upper bound on the total outgassing rate, $\frac{N_T}{\tau}$, is given by (12) directly and is $\sim 4.5 \times 10^{22}$ He atoms sec^{-1}.

This upper bound on the total outgassing rate may also be viewed as the upper bound to thermal loss. The value reported here is substantially less than that given by Broadfoot et al. (1976a) of $3. \times 10^{23} sec^{-1}$. We attribute this difference to large differences in exospheric scale height structure between the models.

This can be seen in the large differences between the model intensities from dayside limb to evening terminator in Broadfoot et al. Figure 2 and our Figure 4. In particular the Broadfoot et al. model shows a much larger bulge in the sunlit region near the terminator. We believe this bulge is unrealistic as it contains model values greater than observed data points which possess surface albedo contributions.

SUMMARY

From a solution of the heat conduction equation over Mercury's surface we have calculated the surface exobase temperatures at aphelion. With these temperatures we have generated normalized exobase densities on the surface via Monte Carlo techniques and computed the normalization factor by comparing model 584 Å intensities with those intensities observed by Mariner 10 at its third Mercury encounter. Using these exobase temperatures and densities we have computed the total atmospheric content and from this value estimated the total magnetospheric capture fraction of solar wind He^{++} needed to maintain the observed exosphere solely by this external source. We found $f_c \sim 4.5 \times 10^{-4}$. An upper bound to the surface outgassing rate of $4.5 \times 10^{22} sec^{-1}$ was also derived. These results represent a synthesis of the data obtained by the UV, IR and magnetic field instruments during Mariner 10's encounters with Mercury. In closing we note once more the sensitivity of the observations to the surface temperature distribution and the corresponding nonlinear amplification of temperature differences in computed model column densities on the nightside near the terminator.

These temperature differences in turn are dependent on the inhomogenieties of the surface properties away from the vicinity of the subsolar point where radiative equilibrium holds. A more refined analysis will most likely require the information that can only be provided by an orbiting spacecraft which would allow detailed observations of the surface temperature at all local times and a wide range of latitudes as well as more detailed density measurements or preferably a lander capable of in situ measurements. This contrasts to the three thin slices of encounter data that Mariner 10 has provided us in our first close-up view of Mercury.

ACKNOWLEDGMENTS

We thank both Lloyd Treinish, a summer student from MIT for programming assistance and D. R. Howell of Goddard Space Flight Center for providing us with the necessary Mariner 10 ephemeris at the third encounter.

REFERENCES

1. Broadfoot, A. L., S. Kumar, M. J. S. Belton, M. B. McElroy, "Mercury's Atmosphere from Mariner 10: Preliminary Results", Science, 185, 166, 1974.

2. Broadfoot, A. L., D. E. Schemansky, S. Kumar, "Mariner 10: Mercury's Atmosphere", Geophys. Res. Letters, 3, 577, 1976a.

3. Broadfoot, A. L., S. S. Clapp, F. E. Stuart, "Mariner 10 Ultraviolet Spectrometer: Airglow Experiment", Space Science Instrumentation, 1976b.

4. Chase, S. C., E. D. Miner, D. Morrison, G. Munch, G. Neugebauer, "Mariner 10 Infrared Radiometer Results: Temperatures and Thermal Properties of the Surface of Mercury", Icarus, 28, 655, 1976.

5. Hartle, R. E., "Model for Rotating and Nonuniform Planetary Exospheres", Phys. Fluids, 14, 2592, 1971.

6. Hartle, R. E., S. A. Curtis, G. E. Thomas, "Mercury's Helium Exosphere", J. Geophys. Res., 80, 3689, 1975.

7. Hartle, R. E., K. W. Ogilvie, C. S. Wu, "Neutral and Ion-Exospheres in the Solar Wind with Applications to Mercury", Planet. Space Sci., 2181, 1973.

8. Hodges, R. R. and J. H. Hoffman, "Measurements of Solar Wind Helium in the Lunar Atmosphere", Geophys. Res. Letters, 1, 69, 1974.

9. Hodges, R. R., "Model Atmospheres for Mercury Based on a Lunar Analogy", J. Geophys. Res., 79, 2881, 1974.

10. Ingrao, H. C., A. T. Young, J. L. Linsky, "A Critical Analysis of Lunar Temperature Measurements in the Infrared", Harvard College Observatory Scientific Report No. 6, 1965.

11. Kumar, S., "Mercury's Atmosphere: A Perspective After Mariner 10", Icarus, 28, 579, 1976.

12. Linsky, J. L., "A Computer Program to Solve the Heat-Conduction Equation in the Lunar Surface for Temperature-Dependent Thermal Properties," Harvard College Observatory Scientific Report No. 7, 1965.

13. Linsky, J. L., "Models of the Lunar Surface Including Temperature-Dependent Thermal Properties", Icarus, 5, 666, 1966.

14. Morrison, D., "Thermal Models and Microwave Temperatures of the Planet Mercury", Smithsonian Astrophysical Observatory Special Report 292, 1969.

15. Morrison, D., "Thermophysics of the Planet Mercury", Space Science Rev., 11, 271, 1970.

16. Ness, N. F., K. W. Behannon, R. P. Lepping, Y. C. Whang, "The Magnetic Field of Mercury: 1", J. Geophys. Res., 80, 2710, 1975.

17. Ness, N. F., K. W. Behannon, R. P. Lepping, Y. C. Whang, K. H. Schatton, "Magnetic Field Observations near Mercury: Preliminary Results from Mariner 10", Science, 185, 151, 1974.

18. Ogilvie, K. W., J. D. Scudder, R. E. Hartle, G. L. Siscoe, H. S. Bridge, A. J. Lazarus, J. R. Asbridge, S. J. Bame, and C. M. Yeates, "Observations at Mercury Encounter by the Plasma Science Experiment on Mariner 10", Science 185, 145, 1974.

19. Richtmyer, R. D., Difference Methods for Initial Value Problems, Interscience Publishers, Inc., N. Y., pp. 91-96, 1962.

20. Siscoe, G. and L. Christopher, "Variations in the Solar Wind Standoff Distance at Mercury", Geophys. Res. Letters, 2, 158, 1975.

Table 1

Heat Conduction Equation Parameters

Parameter	Value
ρ (surface density)	1.50 g cm^{-3}
c (specific heat capacity)	0.20 cal deg^{-1} g^{-1}
K (thermal conductivity)	1.30 x 10^{-5} cal cm^{-1} sec^{-1} deg^{-1}
e (emissivity)	0.90
a (albedo)	0.10
σ (Stephen-Boltzmann constant)	1.35 x 10^{-12} cal cm^{-2} deg^{-4} sec^{-1}

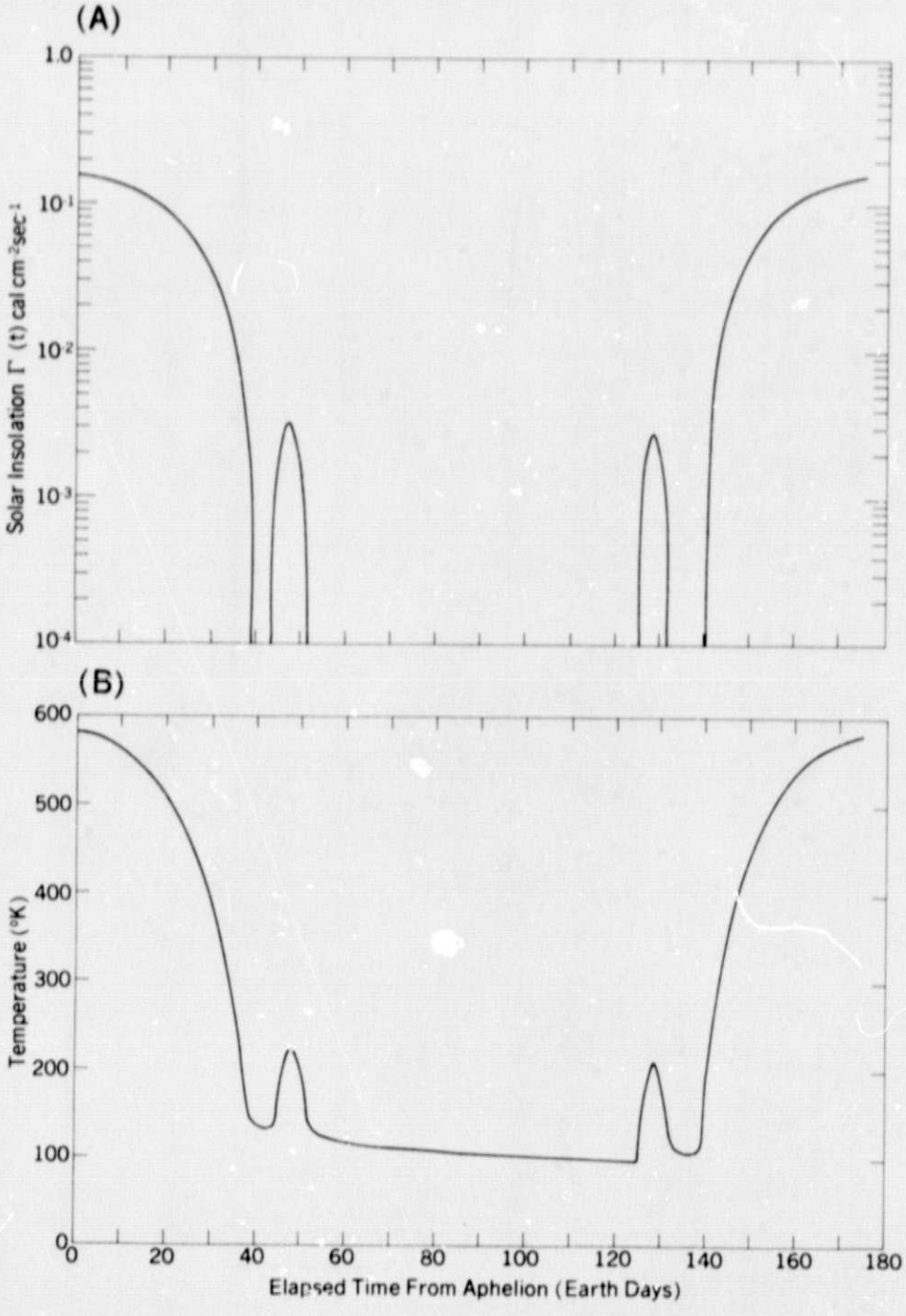

Figure 1 (a) Solar insolation history of the aphelion subsolar point of Mercury as a function of elapsed time from aphelion in earth days. (b) Temperature history of the aphelion subsolar point in Mercury as a function of elapsed time from aphelion in earth days.

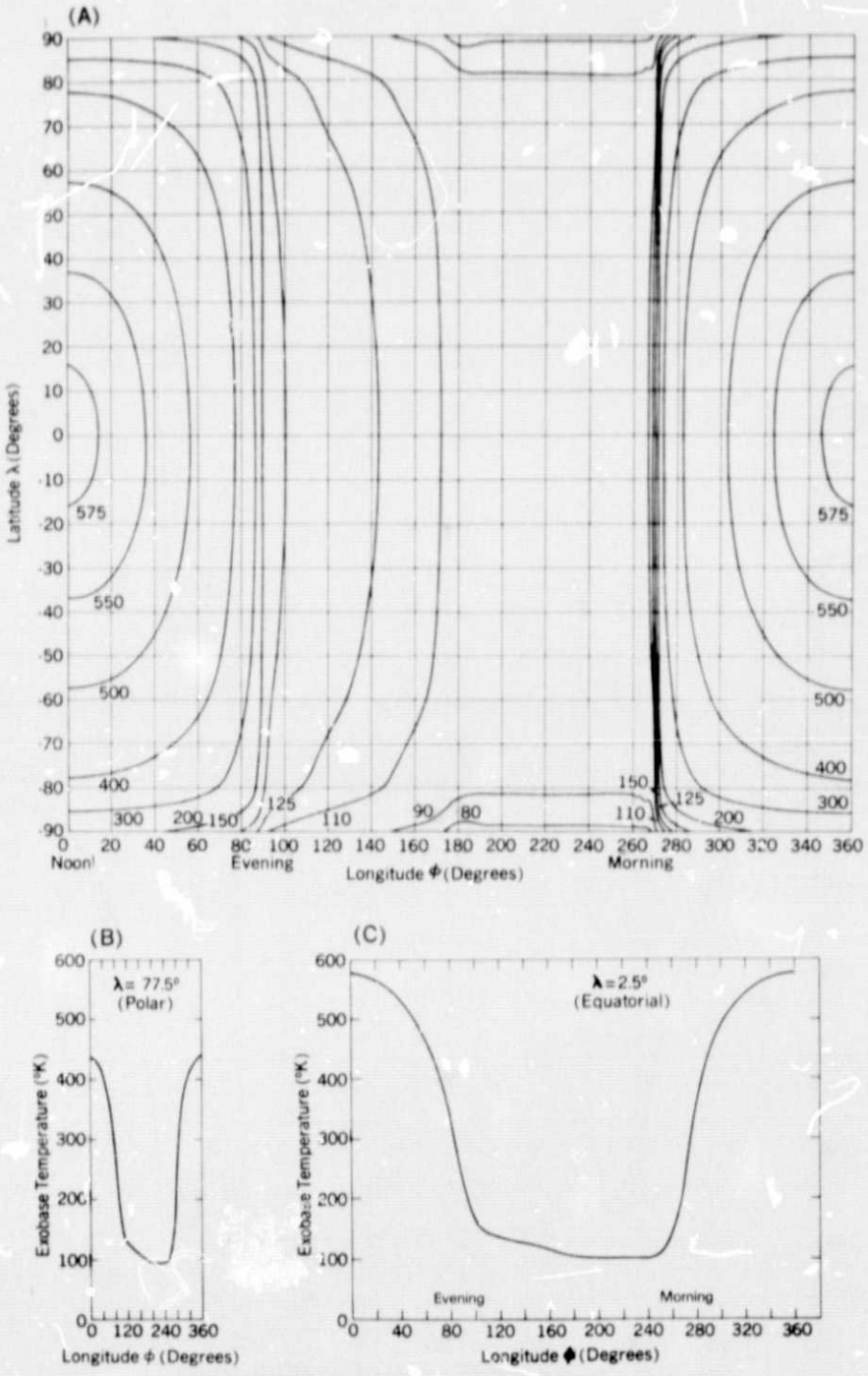

Figure 2 (a) Hermian surface temperature distribution at aphelion as a function of latitude, λ, and longitude, ϕ. (b) Longitudinal cross section of Figure 2 (a) for polar latitude, λ=77.5°. (c) Longitudinal cross section of Figure 2 (a) for equatorial latitude, λ=2.5°.

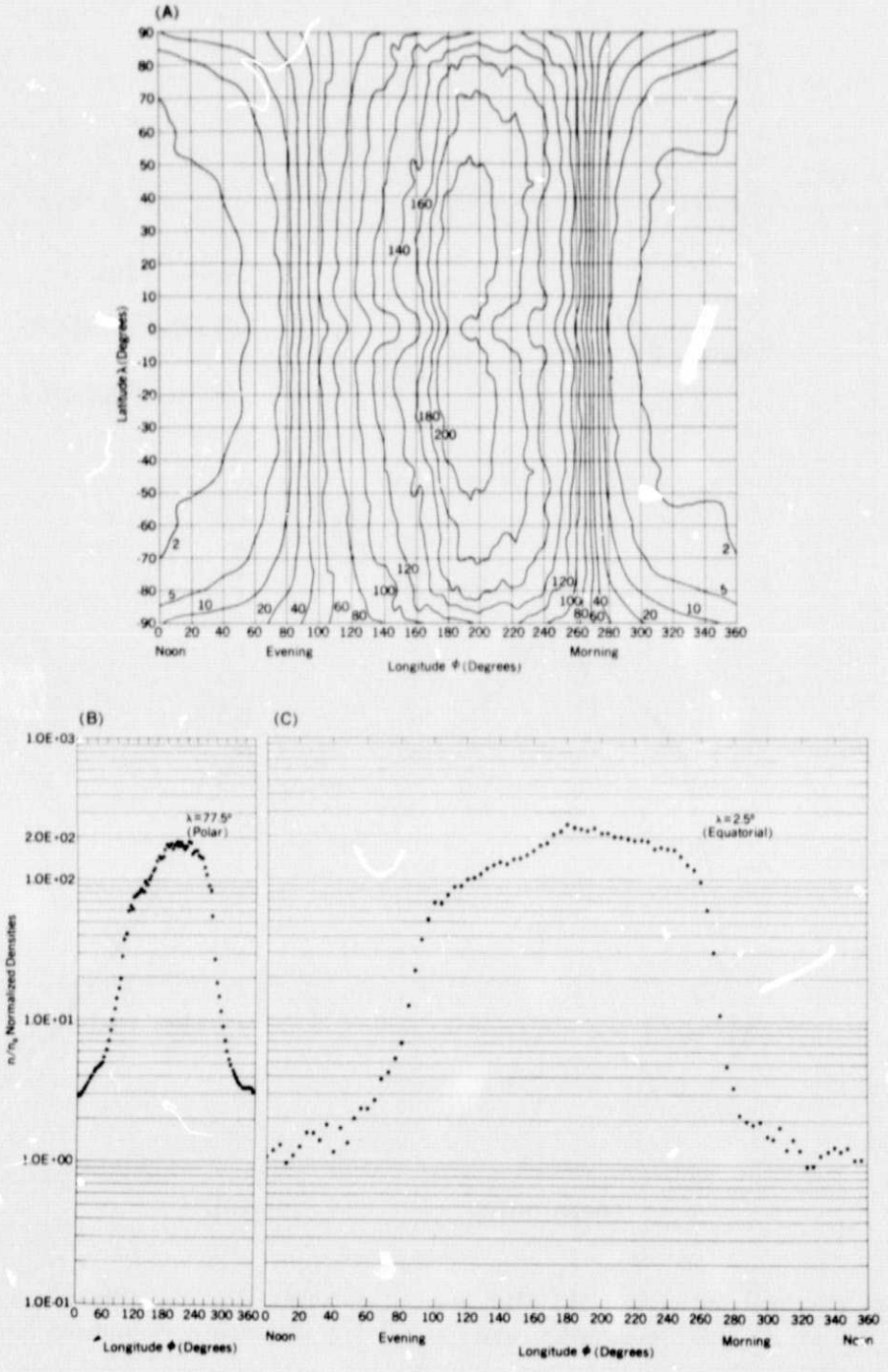

Figure 3 (a) Hermian surface He density at aphelion as a function of latitude, λ, and longitude, ϕ. (b) Longitudinal cross section of Figure 3 (a) for polar latitude, λ=77.5°. (c) Longitudinal cross section of Figure 3 (a) for equatorial latitudes, λ=2.5°.

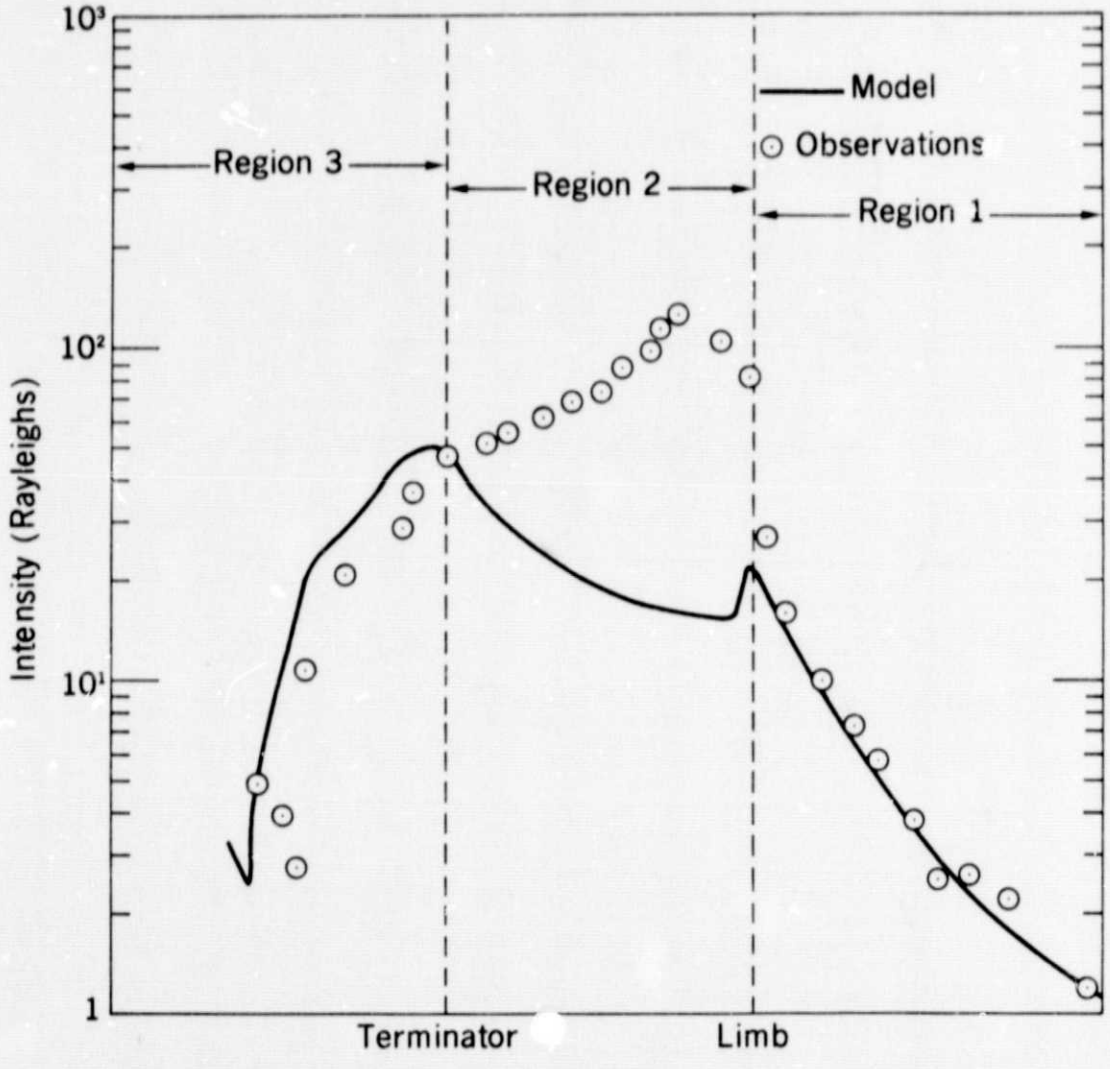

Figure 4 Comparison of the He 584 Å evening terminator intensities observed by Mariner 10 at its third encounter and model He exosphere computed intensities.